Research Article | Vol. 29, No. 5 / 1 March 2021 / Optics Express 6368
Optics EXPRESS

Laser acquisition experimental demonstration for space gravitational wave detection missions

RUIHONG GAO,[1,2,3] HESHAN LIU,[1] YA ZHAO,[4,5] ZIREN LUO,[1,*] JIA SHEN,[1,2] AND GANG JIN[1,2]

[1] *Institute of Mechanics, Chinese Academy of Sciences, Beijing 100190, China*
[2] *School of Engineering Science, University of Chinese Academy of Sciences, Beijing 100049, China*
[3] *School of Fundamental Physics and Mathematical Sciences, Hangzhou Institute for Advanced Study, University of Chinese Academy of Sciences, Hangzhou 310024, China*
[4] *Changchun Institute of Optics, Fine Mechanics and Physics, Chinese Academy of Sciences, Changchun 130033, China*
[5] *School of Optoelectronics, University of Chinese Academy of Sciences, Beijing 100049, China*
[*] *luoziren@imech.ac.cn*

Abstract: The laser acquisition-pointing technique is one of the most important techniques for space gravitational wave detection missions, like the Taiji program and the LISA (Laser Interferometer Space Antenna) program. The laser acquisition system suppresses the laser deviation angle to 1 μrad at the receiving aperture. Corresponding to 80 times of telescope magnification, the acquisition accuracy should reach 80 μrad at the acquisition camera. In order to verify the feasibility of the laser acquisition scheme, a laser acquisition ground simulation experimental system is designed and constructed. The experimental system simulates the actual acquisition process of the Taiji from three aspects: optical path, acquisition accuracy and acquisition scanning process. In the experiment, the coupling between the laser acquisition system and the laser pointing system is considered by introducing the DWS (Differential Wave-front Sensing) technique to calibrate the reference position of the acquisition camera and read out the acquisition precision. Due to limited beam propagation distance in the ground experiment, the in-flat top properties of the transmitting beam will greatly affect the acquisition precision. Based on the analysis of the influence, an improved acquisition ground simulation scheme is introduced. The experimental results indicate that the experimental system can achieve the acquisition accuracy of sub-10 μrad magnitude at the acquisition camera. The experimental system realizes methodological demonstration of the acquisition scheme. The results offer the experimental foundation and theoretical basis for the acquisition system of the Taiji/LISA program.

1. Introduction

The Taiji program [1–3] and the LISA program [4,5] are the most typical space gravitational wave detection missions. They are proposed to detect the gravitational wave signal within the frequency band of 0.1 mHz-1 Hz by inter-satellite laser interferometer. When the satellites launch into the definitive orbit, the science measurement can't be processed immediately because of the limited navigation precision. Therefore, a dedicated laser acquisition-pointing system is introduced to construct a stable inter-satellite laser link. Compared with other missions with inter-satellite laser link, such as the SILEX (Semiconductor Laser Inter-satellite Link Experiment) [6] and the GRACE Follow-on [7–9], gravitational wave detection missions put forward higher requirement for laser acquisition-pointing system. With the satellites separation of 3×10^6 km, the laser acquisition-pointing system should suppress the laser pointing error from 10 mrad magnitude to 1 nrad/$\sqrt{\text{Hz}}$ magnitude under weak laser intensity condition. As a result, a scheme with three stage detectors is proposed [10–12]. Firstly, STRs (Star Trackers) with wide FOV

#414741 https://doi.org/10.1364/OE.414741
Journal © 2021 Received 12 Nov 2020; revised 8 Feb 2021; accepted 9 Feb 2021; published 16 Feb 2021

Optics EXPRESS

(Field of View) are used to preliminarily suppress the laser pointing error. Then, in the so-called laser acquisition phase, CCD/CMOS acquisition cameras, which have smaller FOV and higher sensitivity, are used to further suppress the laser pointing error. For detecting the gravitational wave signal, the laser pointing jitter should be kept at 1 nrad/$\sqrt{\text{Hz}}$ magnitude. QPD (Quadrant Photodiode) detectors are used in the laser pointing process to fulfill the requirement.

The most critical step of the laser acquisition process is as follows [10]: After STR initial pointing, the remote satellite is sited within an uncertainty cone whose half angle is about 20 μrad [12]. The satellites on both sides of the laser link are defined as SC1 and SC2. At the beginning, SC1 is the laser receiving satellite while SC2 acts as the laser transmitting satellite. Firstly, SC1 keeps staring into its reference direction, while SC2 performs a scanning maneuver to cover the whole uncertainty cone of SC1. At a certain time, the acquisition camera of SC1 can receive the laser signal with enough intensity. When the line of sight of the satellite coincides with the direction of the receiving beam, the laser spot is sited at the reference position of the CMOS, which can be calibrated before launch. As shown in Fig. 1, the offset between the position of the receiving laser spot and the reference position in pitch and yaw direction is proportional to the angle deviation in the corresponding direction. Therefore, by positioning the laser spot center precisely, the laser pointing error can be calculated. With the above results, SC1 can adjust its line of sight and point to SC2. At this time, the CMOS of SC2 can also receive a laser spot. The attitude of SC2 can be adjusted with the same method. The above laser acquisition process intends to suppress the laser pointing error to 1 μrad and make the laser beam enter the FOV of the QPD. After laser frequency scanning, the QPD can receive the interference signal continuously. Then, in the laser pointing phase, the DWS technique is introduced to read the angular deviation precisely [13–16]. The laser pointing jitter is kept at 1 nrad/$\sqrt{\text{Hz}}$ magnitude through feedback control.

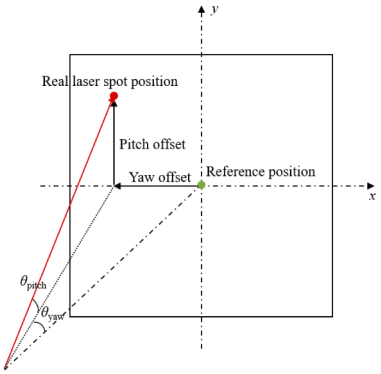

Fig. 1. Diagram of the real laser spot on the acquisition camera surface. The offset angle in the yaw and pitch direction is proportional to the offset distance between real spot position and the reference position in the corresponding direction.

For such a challenging problem, extensive simulations have been performed. T T Hyde introduced the dynamic model of satellite to simulate the acquisition process between two satellites [17]. The simulation results preliminarily verified the feasibility of the two-way laser acquisition scheme of LISA. P G Maghami considered the construction process of three two-way laser links and simulated the whole laser acquisition process of LISA [18]. Francesca Cirillo considered the design of acquisition controller in his thesis [10]. For fulfilling the requirement of LISA, a Kalman filter was introduced. However, the researches on laser acquisition system mainly focused on theoretical demonstration, the simulation results still need to be confirmed by experiments. In this paper, we experimentally demonstrate the laser acquisition system with

Optics EXPRESS

Taiji-like parameters. As the distance between two Taiji satellites is as far as 3×10^6 km, the laser beam at the receiving aperture has the characters of a flat top beam rather than a Gaussian beam while the receiving laser power is as weak as 100 pW magnitude. These actual factors are considered in the experimental system design. On the other hand, although the whole laser link construction process is divided into laser acquisition phase and laser pointing phase, the two phases have strong coupling. Therefore, the coupling is also considered in our experiment.

The manuscript is organized as follows: section 2 introduces the design of the experimental parameters and the experimental setup. In section 3, we analyse the limiting factor of the acquisition precision in the experiment and propose an improved acquisition scheme. In section 4, the laser acquisition experiment is carried out. The results are also shown. A summary of the experiment outcomes is given in section 5.

2. Experimental design

The laser acquisition experimental system is performed as realist as possible. The simulation of the actual process mainly includes the following aspects: (1) acquisition optical system. (2) acquisition precision. (3) acquisition process.

2.1. Acquisition optical system simulation

Each satellite of the Taiji program has an identical optical platform, which contains all the elements of the laser acquisition-pointing system. When the satellite is used for laser transmitting, the laser beam passes through a telescope after reflecting by the PAAM (Point Ahead Angle Mechanism) system. When the satellite is used for laser receiving, the receiving laser beam is firstly clipped by the telescope. Then it is divided into two beams and transmits to acquisition cameras as well as QPDs respectively. According to the laser spot positioning results of the acquisition camera in the acquisition phase, the satellite attitude is adjusted to make the laser beam enter the FOV of the QPDs. Then the DWS signal is read by the QPDs in the laser pointing phase. Our experiment is carried out to simulate the above optical system functions.

Figure 2 presents the diagram of the laser acquisition experimental optical system. The optical system restores nearly all the functions of actual laser acquisition system. In the simulation experiment, platform 1 (P1) will be carried on the P-915k625 hexapod displacement platform of PI company to simulate the laser receiving satellite, while platform 2 (P2) mainly simulates the scanning process of laser transmitting satellite by a FSM (Fast Steering Mirror) constructed from the S-330.2SL piezoelectric deflection platform of PI. The output laser is firstly divided into two beams. The two beams are modulated by AOMs (Acoustic Optical Modulator) to produce a frequency difference for the interference signal. One of the beams is transmitted to P2 through a FC (fiber collimator) (the blue beam in Fig. 2). Then it is reflected by the FSM to the aperture of P1. The FSM can be used to simulate the beam scanning process. After clipping by the aperture, the beam enters the optical system of P1. The beam is divided by a BS (Beam Splitter) and transmits to the SH640 CMOS acquisition camera of TEKWIN company as well as the GD4542-20M QPD of CETC (China Electronic Technology Corporation) respectively. Before entering the CMOS camera, the beam passes through an imaging system and an attenuator. The imaging lens is mainly used to control the spot size on the CMOS surface and ensure the spot quality. We use the attenuator to adjust the laser intensity on the CMOS surface for simulating actual weak receiving intensity condition. Another beam (the red beam in Fig. 2) transmits to the FC on P1 and interferes with the beam transmitted from P2. The interference signal is detected by the QPD. Then, a phasemeter is used to read out the DWS signal, which is the core measurement signal in the laser pointing process. Such design establishes the coupling between laser acquisition system and laser pointing system. As the DWS technique has high angular measurement precision, it can realize the calibration of the CMOS reference position as well as verification of the laser acquisition precision in the experiment.

Optics EXPRESS

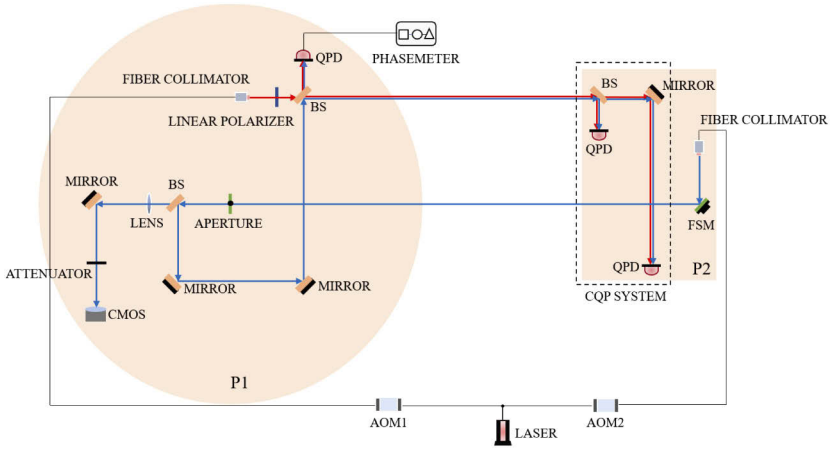

Fig. 2. Diagram of the laser acquisition experimental optical system.

Coincidence degree of the two interference laser beams will influence the readout accuracy of DWS signal by affecting the interference efficiency. Therefore, in addition to beam transmitting devices, P2 also carries a CQP (Calibrated Quadrant Photodiode Pair) auxiliary assembly system. The CQP system is widely used in LISA Pathfinder and other projects for calibrating laser interferometer precisely [19,20]. It consists of two QPDs, a BS and a mirror. The QPDs are mounted at different distances from the BS so that there is a unique optical beam which can simultaneously centred on both detectors. When both of the two interference beams enter center of the two QPDs, the beams are regarded as coincident. Suppose the optical path length difference from the BS to the two QPDs is L_{QPD}, the laser spot positioning precision is x_{QPD}, the deviation angle of the beams after CQP calibrating can be written as x_{QPD}/L_{QPD}. With the above experimental setup, the deviation angle after calibration is estimated as 50 μrad. As the angular dynamic range of the hexapod is $\pm$700 μrad, the residual angle error can be further suppressed.

2.2. Acquisition precision simulation

The Taiji/LISA program requires that the laser acquisition precision should be higher than 1 μrad at the receiving aperture. The telescope of the Taiji program is a four-mirror off-axis reflection system, whose magnification is 80. With the size of the receiving laser beam decreases 80 times, the laser pointing error increases 80 times at the same time. Therefore, the requirement of acquisition precision at the acquisition camera is 80 μrad. In the Taiji program, the wavefront distortion of the telescope should be kept within $\lambda/30$. The imperfect telescope will influence the acquisition precision from two aspects. Firstly, telescope aberration will cause the deviation of the transmitting optical axis and the receiving optical axis. On the other hand, the aberration will change the laser spot intensity distribution on the CMOS detector. As the laser center positioning is based on the centroid method, the aberration will also influence the acquisition precision by causing spot positioning error. With no telescope system in the experiment, the following aspects won't influence the acquisition precision. Therefore, the acquisition precision of 80 μrad is set as the target precision.

2.3. Acquisition process simulation

The core process of the laser acquisition phase is introduced in section 1. In the experiment, such process is restored as truly as possible. As introduced in section 2.1, The included angle between the laser beam from P2 and the local laser beam of P1 is of 10 μrad magnitude after assembling

Optics EXPRESS

the optical system in Fig.2. Then we adjust the attitude of the hexapod to make the DWS signal equal to zero. At this time, the laser spot position on the CMOS is calibrated as the reference position with the help of an improved centroid method, which has the potential to be used in the Taiji program [21]. By changing the attitude of the hexapod, the angle-position conversion coefficient of the CMOS and the phase-angle conversion coefficient of the DWS signal can also be calibrated. After the calibration phase, P1 and P2 will be moved to an arbitrary position within the dynamic range of the hexapod. The FSM on P2 scans over the area of P1 following a scanning pattern. The constant tangential speed Archimedean spiral scanning pattern is used in the experiment because of its advantage of uniformity. When the CMOS camera receives the laser signal with enough power, center position of the laser spot can be calculated. Similar with the actual acquisition process, the attitude of P1 is adjusted based on the difference between the measurement position and the reference position. Finally, the acquisition precision is readout by the DWS signal.

In actual condition, the far field wavefront has the properties of spherical wave while the intensity distribution at the receiving aperture has the properties of plane wave because of the large difference between the receiving beam diameter and the telescope diameter. As a result, the receiving laser beam at the remote satellite is a flat top beam. The current laser acquisition method is practicable only with a flat top beam. Therefore, in order to guarantee the above process running smoothly, the far field wavefront simulation is the most important factor. We define the flat top beam approximate coefficient m_{flat} as the ratio of the laser diameter at the receiving aperture D_{div} to the diameter of the aperture D_{tel}. For the Taiji program, the value of m_{flat} is as big as 30667. The bigger the m_{flat}, the closer the laser beam is to a flat top beam. In the laser acquisition experiment, m_{flat} can be written as,

$$m_{flat} = \frac{\sqrt{\omega_0^2 + \frac{\lambda^2 z^2}{\pi^2 \omega_0^2}}}{\varepsilon}, \tag{1}$$

where, ω_0 is the waist radius of the Gaussian beam on P2, λ is the wavelength, z is the transmitting distance from the fiber collimator of P2 to the aperture of P1 and ε is the radius of the aperture. We differentiate m_{flat} with respect to ω_0 and achieve,

$$\frac{\partial m_{flat}}{\partial \omega_0} = \frac{1}{\varepsilon}(\omega_0^2 + \frac{\lambda^2 z^2}{\pi^2 \omega_0^2})^{-\frac{1}{2}} \cdot (\omega_0 - \frac{\lambda^2 z^2}{\pi^2 \omega_0^3}). \tag{2}$$

From formula (1) and formula (2), we can conclude that m_{flat} increases with the increase of z and the decrease of ε while m_{flat} decreases firstly then increases with increment of ω_0. When $\omega_0 = \sqrt{\lambda z/\pi}$, m_{flat} takes the minimum value. As the laser transmitting distance z is limited in the ground-based experiment, an aperture with small diameter is used to replace the actual telescope system in the experiment.

For simulating the scanning process, the scanning range is also considered. We define the scanning range coefficient n_{scan} as the ratio of the uncertainty cone radius at the receiving aperture R_{uc} to the radius of the laser beam. For the Taiji program, $n_{scan} \approx 16.8$. In the experiment, n_{scan} can be written as,

$$n_{scan} = \frac{\alpha}{\sqrt{\frac{\omega_0^2}{z^2} + \frac{\lambda^2}{\pi^2 \omega_0^2}}}, \tag{3}$$

where, α is the scanning rang of the FSM. We differentiate n_{scan} with respect to ω_0 and achieve,

$$\frac{\partial n_{scan}}{\partial \omega_0} = -\alpha\omega_0(\frac{\omega_0^2}{z^2} + \frac{\lambda^2}{\pi^2 \omega_0^2})^{-\frac{3}{2}} \cdot (\frac{\omega_0^2}{z^2} - \frac{\lambda^2}{\pi^2 \omega_0^2}). \tag{4}$$

Optics EXPRESS

It can be concluded that n_{scan} increases with the increase of z and α while n_{scan} increases firstly then decreases with increment of ω_0. Therefore, the parameters used in the experiment need to be traded off between flat top beam simulation and scanning range. Table 1 presents values of the core parameters in the experiment and the comparison with the Taiji program. As the beam transmitting distance is limited in the experiment, the value of n_{scan} and m_{flat} can hardly be perfectly restored. The smaller n_{scan} will only cause the CMOS detect the laser beam easier. However, the smaller m_{flat} will cause the increment of in-flat top properties of the receiving beam, which may have a great influence to the acquisition process as well as the DWS read-out. The influence is further studied in the next section.

Table 1. Core parameters comparison between the laser acquisition experiment and the Taiji program.

Parameter	Taiji program	Experiment
Platform separation(z)	3×10^6 km	1.5 m
Beam waist radius(ω_0)	30 cm	0.43 mm
Beam radius at receiving aperture($\omega(z)$)	5 km	1.26 mm
Aperture radius(ε)	30 cm	0.4 mm
Scanning range(α)	24 μrad	2 mrad
flat top beam approximate coefficient(m_{flat})	30667	3.2
scanning range coefficient(n_{scan})	16.8	1.2
CMOS FOV(θ_{CMOS})	200 μrad	25.6 mrad
CMOS resolution	640×512 pixel	640×512 pixel

3. Influences of in-flat top properties

As introduced in the last section, with limited laser transmitting distance, the m_{flat} value in ground experiments is much less than the value in actual condition. As a result, the far-field wavefront characters can hardly be well restored. However, the laser acquisition scheme is based on a flat-top beam. Figure 3 presents the near-field wavefront at the receiving aperture. It can be seen that the intensity distribution is in-homogeneity while the beam transmitting direction is in-consistency within the aperture area. The in-flat top properties of the receiving beam may greatly influence the acquisition precision as well as the DWS read-out precision.

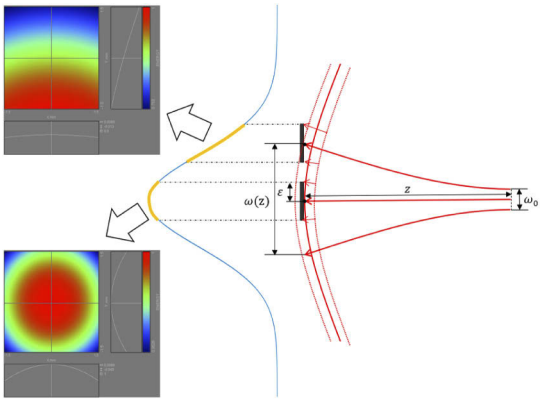

Fig. 3. Diagram of the near-field wavefront at the receiving aperture.

Optics EXPRESS

3.1. Influence of in-flat top properties to the acquisition process

In the laser acquisition process, the laser spot center is positioned based on the centroid method. The laser center position is considered coincident with the centroid position, which is defined as,

$$x = \frac{\sum_{i=1}^{n} x_i N_i}{\sum_{i=1}^{n} N_i}, \qquad y = \frac{\sum_{i=1}^{n} y_i N_i}{\sum_{i=1}^{n} N_i}, \tag{5}$$

where, x_i, y_i denotes the position of the ith pixel, N_i stands for the detected photo events and n is the total pixel number involved in calculation.

If the intensity of the laser spot has symmetrical distribution, the spot centroid position well coincides with its center position. A flat top beam has uniform distribution, so the centroid method works well in actual condition. However, in the laser acquisition experiment, the intensity distribution of the laser spot is no longer symmetrical except when the aperture is seated at the center of the receiving laser beam. As shown in Fig.3, if the aperture is seated at the edge of the receiving laser beam, the detected centroid position deviates from the spot center. It will greatly influence the acquisition precision.

To estimate the impact, we only consider the FC, the aperture as well as the CMOS/QPD detector and simplify the model of the experimental system as shown in Fig. 4, where the red line refers to the transmitting direction of the laser beam. Here, the transmitting beam only deviates in the pitch direction (the deviation in the yaw direction comes to the same conclusion). Where, L_1 represents the distance between the FC and the aperture, L_2 represents the distance between the aperture and the QPD, L_3 represents the distance between the aperture and the CMOS, ε stands for the radius of the aperture, φ is the deviation angle in the pitch direction. Figure 4(a) presents the condition of far-field flat top beam incidence. After passing through the aperture, the incidence beam is similar with a plane wave beam. At this time, the centroid position approximately coincides with the center of the laser spot, which can be written as,

$$y_{center-flat} = y_{ref} - L_2 \cdot \varphi, \tag{6}$$

where, y_{ref} denotes the reference position in the y-direction.

Similar with the experimental parameters, we firstly suppose that L_1 =1 m, L_3 =0.25 m, ε = 0.4 mm, $y_{reference}$ =256 pixel. With the formula (6), the blue curve in Fig. 5(a) presents the relationship between the deviation angle and the spot centroid position with flat top beam incidence. Figure 4(b) and Fig. 4(c) present the near-field Gaussian beam incidence condition, with the only difference of the laser transmitting direction. In Fig. 4(b), the Gaussian beam normal incidents to the aperture. We use the optical simulation software ASAP to simulate the intensity distribution on the CMOS surface. With the above parameters, Fig. 6(a) presents the intensity distribution with the deviation angle of 700 μrad. It can be seen that the intensity distribution is in-homogeneity in the y-direction. Then we use the centroid method for various deviation angle conditions. The red curve in Fig. 5(a) shows the relationship between the deviation angle and the spot centroid position with Gaussian beam normal incidence. By comparing the red curve and the blue curve in Fig. 5(a), it can be seen that the center positioning error increases to 100 μrad magnitude with the increasing of the deviation angle when the Gaussian beam normal incident to the aperture. Fig. 5(b) presents the corresponding results with only L_1 changing to 10 m. The offset between the blue cure and the red curve greatly reduces while the center positioning error for Gaussian beam incidence reduces as well. Therefore, the laser acquisition method is greatly influenced in near-field condition even with the radius of the aperture as small as 0.4 mm.

The influence is mainly due to the near-field asymmetric distribution of laser intensity. To reduce the influence, we consider the condition of Fig. 4(c), in which the Gaussian beam oblique incidents with the beam pointing to the center of the aperture. With the same model parameters used for Fig. 6(a), Fig. 6(b) also presents the intensity distribution with the deviation angle of

Optics EXPRESS

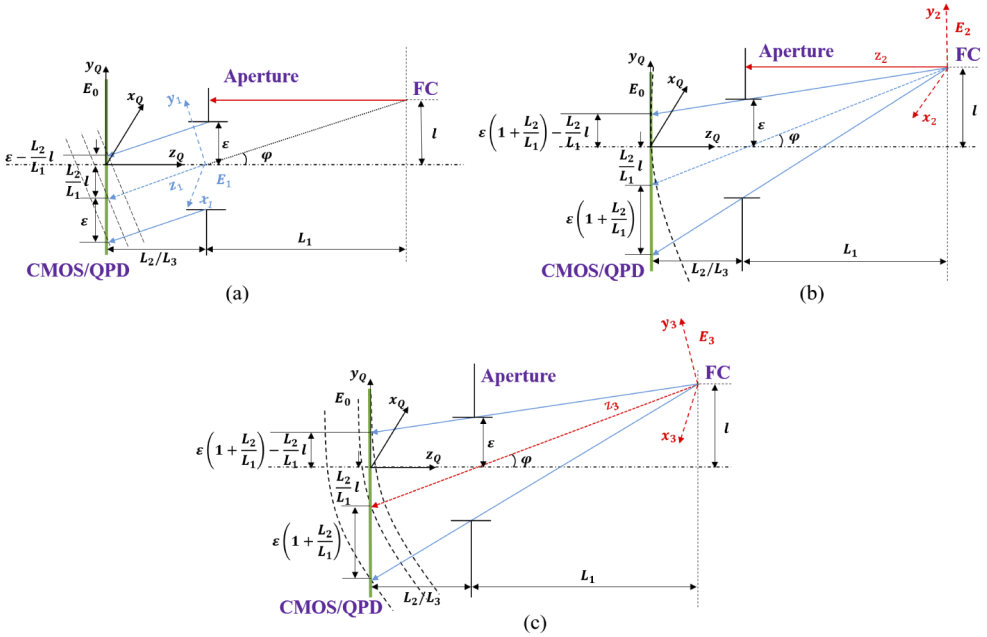

Fig. 4. Diagram of the simplified models of the laser acquisition experimental optical system. Where, (x_Q, y_Q, z_Q) is the coordinate of the QPD. (a) The condition of the flat top beam incidence, where (x_1, y_1, z_1) is the coordinate of flat top beam. (b) The condition of the Gaussian beam normal incidence, where (x_2, y_2, z_2) is the coordinate of Gaussian beam. (c) The condition of the Gaussian beam oblique incidence to the center of the aperture center, where (x_3, y_3, z_3) is the coordinate of Gaussian beam.

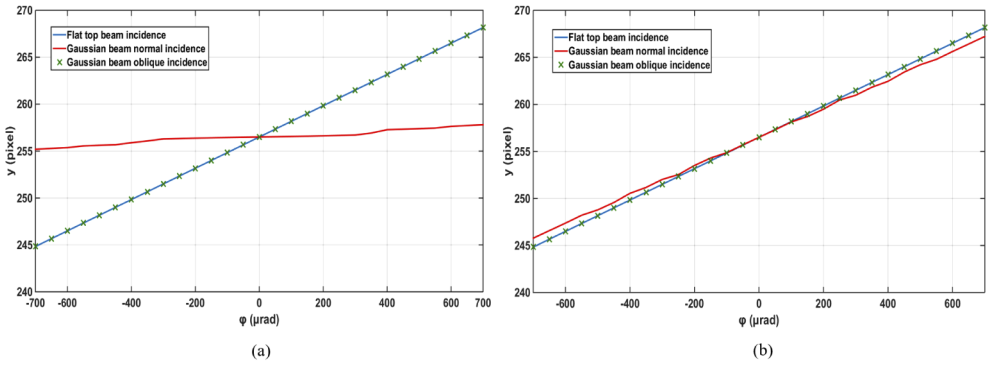

Fig. 5. The numerical result of the relationship between the deviation angle and the laser spot centroid position on the CMOS. Blue curve: with flat top beam incidence. Red curve: with Gaussian beam normal incidence. Green curve: with Gaussian beam oblique incidence. (a) L_1 =1 m. (b) L_1 =10 m.

Optics EXPRESS

700 μrad. Compared with Fig. 6(a), the symmetry distribution is better. The green curves in Fig. 5 shows the spot center positioning results with various deviation angles. It can be seen that the positioning results with Gaussian beam oblique incidence well correspond to the results with flat top beam incidence. The corresponding angular measurement error is smaller than 1μrad.

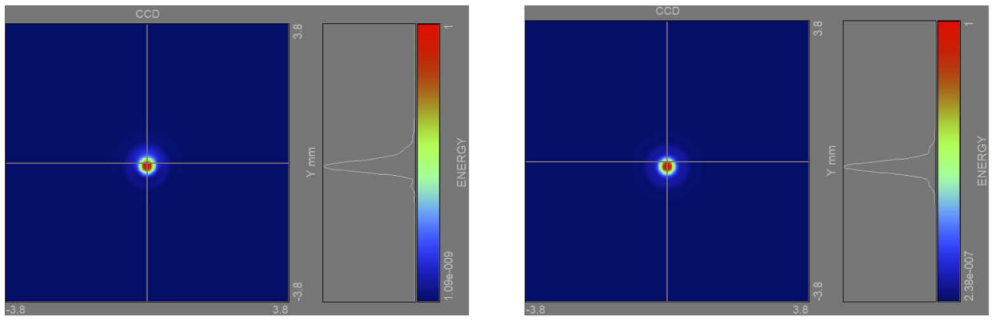

(a) (b)

Fig. 6. The intensity distribution with the deviation angle of 700 μrad. (a) Gaussian beam normal incidence. (b) Gaussian beam oblique incidence.

3.2. *Influence of in-flat top properties to the DWS signal*

As the DWS signal is generated from the phase of the interference signal, the in-flat top properties of the receiving beam will affect the read-out precision of the DWS signal as well. To estimate the impact, we construct numerical modules for Figs. 4(a)–4(c). As the P1 platform local Gaussian beam incidents vertically to the QPD center, it can written as,

$$E_0(x,y,z) = \frac{A_0}{\omega(z_0)} exp(-\frac{x^2+y^2}{\omega^2(z_0)}) \cdot exp\left\{-i[k(z_0 + \frac{x^2+y^2}{2R(z_0)}) - \phi(z_0)]\right\}, \tag{7}$$

where z_0 is the laser propagation distance, $\omega(z_0)$ is the laser radius, $R(z_0)$ is the beam radius of curvature, $\phi(z_0)$ is the Gouy phase. The incident beams in Figs. 4(a)–4(c) can be respectively expressed as,

$$E_1(x_1,y_1,z_1) = A_1 exp(-ikz_1), \tag{8}$$

$$E_2(x_2,y_2,z_2) = \frac{A_2}{\omega(z_2)} exp(-\frac{x_2^2+y_2^2}{\omega^2(z_2)}) \cdot exp\left\{-i[k(z_2 + \frac{x_2^2+y_2^2}{2R(z_2)}) - \phi(z_2)]\right\}, \tag{9}$$

$$E_3(x_3,y_3,z_3) = \frac{A_3}{\omega(z_3)} exp(-\frac{x_3^2+y_3^2}{\omega^2(z_3)}) \cdot exp\left\{-i[k(z_3 + \frac{x_3^2+y_3^2}{2R(z_3)}) - \phi(z_3)]\right\}. \tag{10}$$

To derive the expression of the interference signal, the above expressions of the incident light should be transformed to the (x_Q, y_Q, z_Q) coordinate. The transformation formulas can be respectively written as,

$$\begin{pmatrix} x_1 \\ y_1 \\ z_1 \\ 1 \end{pmatrix} = \begin{pmatrix} -1 & 0 & 0 & 0 \\ 0 & cos\varphi & -sin\varphi & L_3 sin\varphi \\ 0 & -sin\varphi & -cos\varphi & L_3 cos\varphi \\ 0 & 0 & 0 & 1 \end{pmatrix} \begin{pmatrix} x_Q \\ y_Q \\ z_Q \\ 1 \end{pmatrix}, \tag{11}$$

Optics EXPRESS

$$\begin{pmatrix} x_2 \\ y_2 \\ z_2 \\ 1 \end{pmatrix} = \begin{pmatrix} -1 & 0 & 0 & 0 \\ 0 & 1 & 0 & -l \\ 0 & 0 & -1 & L_1+L_2 \\ 0 & 0 & 0 & 1 \end{pmatrix} \begin{pmatrix} x_Q \\ y_Q \\ z_Q \\ 1 \end{pmatrix}, \tag{12}$$

$$\begin{pmatrix} x_3 \\ y_3 \\ z_3 \\ 1 \end{pmatrix} = \begin{pmatrix} -1 & 0 & 0 & 0 \\ 0 & cos\varphi & -sin\varphi & lcos\varphi + (L_1+L_2)sin\varphi \\ 0 & -sin\varphi & -cos\varphi & -lsin\varphi + (L_1+L_2)cos\varphi \\ 0 & 0 & 0 & 1 \end{pmatrix} \begin{pmatrix} x_Q \\ y_Q \\ z_Q \\ 1 \end{pmatrix}. \tag{13}$$

For the conditions in Fig. 4, only the DWS signal of the up and down quadrant is considered (the right and left quadrants DWS signal equals to zero when the transmitting beam only deviates in the pitch direction). Therefore, without considering the diffraction effect, the complex amplitude of the interference pattern on the up and down quadrant of the QPD is given by,

$$F_{up,i} = \int_{S_{up}} E_0 E_i'^{*} \cdot dS, \qquad F_{down,i} = \int_{S_{down}} E_0 E_i'^{*} \cdot dS, \tag{14}$$

where $E_i'(i = 1, 2, 3)$ stands for the expression of E_i written in the (x_Q, y_Q, z_Q) coordinate, S_{up} and S_{down} stand for the integral area of the up and down quadrant respectively. Then the DWS signal can be given by $DWS_i = arg(F_{up,i}/F_{down,i})$. After substituting formula (7) – (13) into formula (14), the DWS signal can be written as,

$$DWS_1 = arg\left\{ \frac{\int_0^{\varepsilon - \frac{L_2}{L_1}l} exp[-\frac{y^2}{\omega^2(z_0)} - ik(\frac{y^2}{2R(z_0)} + ysin\varphi)]dy}{\int_{-\varepsilon-\frac{L_2}{L_1}l}^{0} exp[-\frac{y^2}{\omega^2(z_0)} - ik(\frac{y^2}{2R(z_0)} + ysin\varphi)]dy} \right\}, \tag{15}$$

$$DWS_2 = arg\left\{ \frac{\int_0^{\varepsilon(1+\frac{L_2}{L_1})-\frac{L_2}{L_1}l} exp[-\frac{y^2}{\omega^2(z_0)} + \frac{y^2-2ly}{\omega^2(L_1+L_2)} - ik(\frac{y^2}{2R(z_0)} - \frac{y^2-2ly}{2R(L_1+L_2)})]}{\int_{-\varepsilon(1+\frac{L_2}{L_1})-\frac{L_2}{L_1}l}^{0} exp[-\frac{y^2}{\omega^2(z_0)} + \frac{y^2-2ly}{\omega^2(L_1+L_2)} - ik(\frac{y^2}{2R(z_0)} - \frac{y^2-2ly}{2R(L_1+L_2)})]} \right\}, \tag{16}$$

$$DWS_3 = arg\left\{ \frac{\int_0^{\varepsilon(1+\frac{L_2}{L_1})-\frac{L_2}{L_1}l} exp[-\frac{y^2}{\omega^2(z_0)} + \frac{y_0^2}{\omega^2(L_1+L_2)} - iky_1] - ikysin\varphi]}{\int_{-\varepsilon(1+\frac{L_2}{L_1})-\frac{L_2}{L_1}l}^{0} exp[-\frac{y^2}{\omega^2(z_0)} + \frac{y_0^2}{\omega^2(L_1+L_2)} - iky_1] - ikysin\varphi]} \right\}, \tag{17}$$

where,

$$y_0 = (y + l)cos\varphi + (L_1 + L_2)sin\varphi, \tag{18}$$

$$y_1 = \frac{y^2}{2R(z_0)} - \frac{y_0^2}{2R(L_1 + L_2)}. \tag{19}$$

With the numerical method and the above expressions, we can achieve the relationship between the deviation angle and the DWS signal of various conditions. We firstly suppose that L_1 =1 m, L_2 =0.5 m, ε =0.4 mm. The parameters are similar with those used in the experiment. Figure 7(a) shows the numerical results. Compared with the DWS signal with the flat top beam incidence, the DWS signal with the near-field Gaussian beam incidence has an offset. Then we reduce the in-flat top properties by changing the value of L_1 to 10 m (the results are presented in Fig. 7(b)). It can be seen that the offset greatly reduced. As a result, the in-flat top property influences the DWS read out precision as well.

Optics EXPRESS

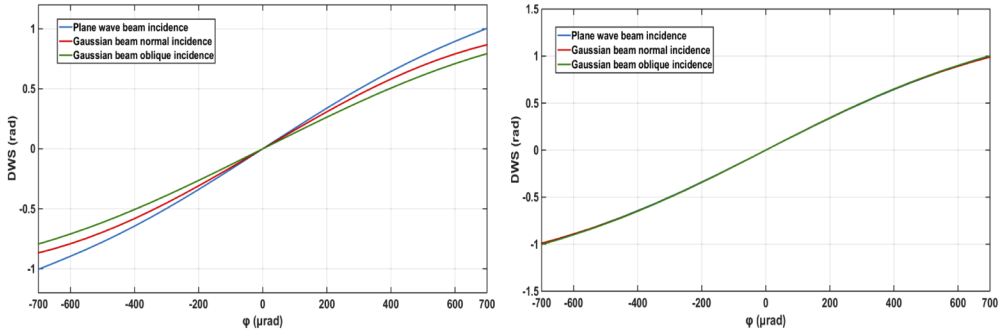

Fig. 7. The numerical result of the relationship between the deviation angle and the DWS signal. Blue curve: with flat top beam incidence. Red curve: with Gaussian beam normal incidence. Green curve: with Gaussian beam oblique incidence. (a) L_1 =1 m. (b) L_1 =10 m.

As the deviation angle is expected smaller than 80 μrad after laser acquisition experiment, Fig. 8 shows the DWS read out error within ±80 μrad. We can conclude that the read out error increases with the increase of the deviation angle φ. On the other hand, no matter how the Gaussian beam incidence, the DWS read out error is smaller than 20 μrad, which is better than the acquisition precision requirement of 80 μrad.

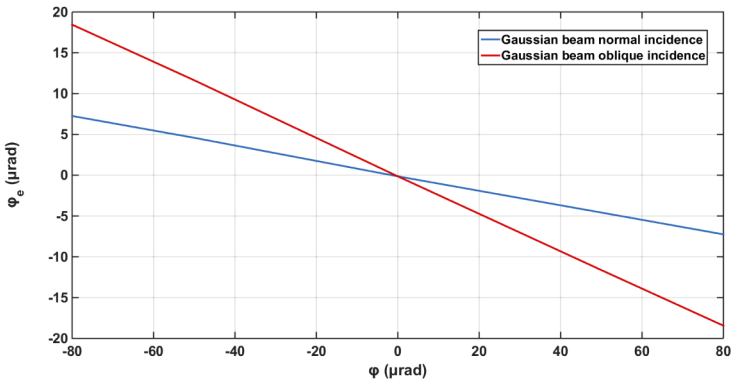

Fig. 8. The DWS read out error within $\varphi \in (-80\mu\text{rad}, 80\mu\text{rad})$. Blue curve: with Gaussian beam normal incidence. Red curve: with Gaussian beam oblique incidence. Where, $L_1 = 1m$.

3.3. Acquisition schemes

In the actual condition of the Taiji, the acquisition process is carried out whenever the CMOS camera receives enough laser power. At this time, the direction of the receiving beam is arbitrary within the uncertainty cone (Fig. 4(b) is an example). It is called the direct acquisition scheme.

Based on the above analysis, for achieving higher acquisition precision in the laser acquisition experiment, an effective method is to make the transmitting laser beam point to the center of the aperture before carrying out the acquisition process. Therefore, a scan-pointing acquisition scheme is introduced as follows. At first, by adjusting the attitude of the FSM, the transmitting laser beam scans over the whole uncertainty cone of the P1 platform. Meanwhile, the CMOS camera collects the laser spot pictures and calculates the total photo-electron numbers continuously. At a certain time, the transmitting beam points to the center of the aperture. The CMOS receives the

Optics EXPRESS

maximum laser power at this time. Therefore, after completing the whole scanning process, the moment when the transmitting beam points to the aperture center (the condition of Fig. 4(c)) can be found by retrieving the picture with the maximum photo-electron numbers. Then we can adjust the laser beam pointing to the corresponding direction. The attitude of the hexapod is adjusted with the laser spot center positioning result at this time.

In the experiment, both direct acquisition scheme and scan-pointing acquisition scheme are carried out. Theoretically, better acquisition precision can be achieved with scan-pointing acquisition scheme.

4. Experimental result

In section 2, we present the details of the experimental design. Fig. 9 presents the physical map of the laser acquisition experimental setup. As introduced in section 2.3, the calibration process is firstly carried out in the experiment. Then we experiment the laser acquisition process.

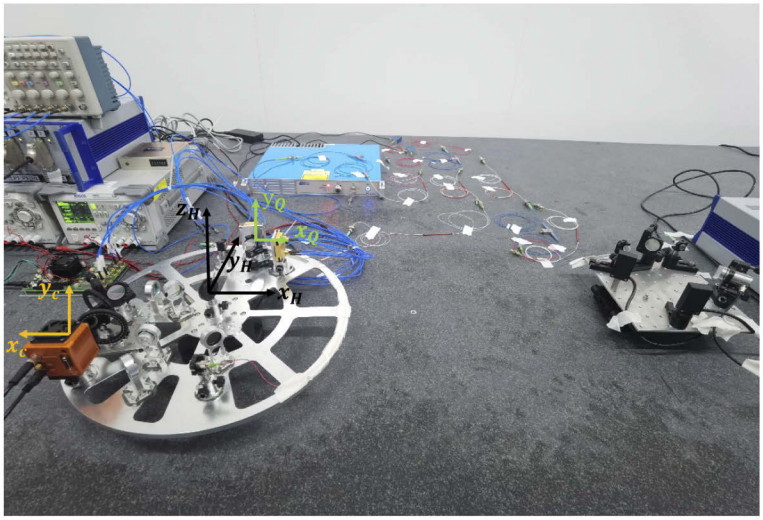

Fig. 9. Physical map of the laser acquisition experimental setup. Where (x_H, y_H, z_H) is the rotation coordinate of the hexapod, (x_C, y_C) is the coordinate of the CMOS surface, (x_Q, y_Q) is the coordinate of the QPD surface.

4.1. Reference position calibration

After assembling, the included angle between the local laser beam of P1 and the receiving laser beam is of 10 μrad magnitude with the help of the CQP system. We adjust the attitude of the hexapod to make the DWS signal equal to zero. At this time, the laser spot image collected by the CMOS camera is shown in Fig. 10(a). The laser power at the CMOS detector is attenuated to 1 nW magnitude for simulating weak receiving light condition. Testing of weaker laser intensity requires a better acquisition camera. The center position of the main laser spot is regarded as the reference position (x_{ref}, y_{ref}). The two smaller laser spot is generated by the second reflection of the attenuators. Same as the actual process, an improved centroid laser spot center positioning method is used in the experiment. The laser center position is calculated with formula (5).

For avoiding the influence of the second reflection spots and improving positioning precision, the improved centroid method only involves the pixels near the main laser spot into calculation. We collect more than 10000 pictures and calculate the mean value as the reference position. The reference position is $(x_{ref}, y_{ref}) = (355.79\text{pixel}, 219.60\text{pixel})$. Make the y-direction as an

Optics EXPRESS

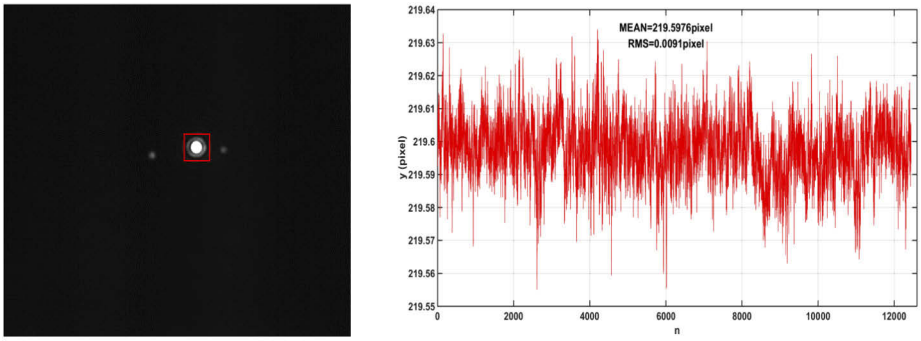

(a) (b)

Fig. 10. (a) Diagram of the laser spot at the reference position. (b) The laser spot center positioning results in he y-direction of the reference position.

example, the results are shown in Fig. 10(b). The RMS (Root Mean Square) value is $0.0091 pixel$, which is much smaller than the requirement of $0.1 pixel$ [12].

4.2. Conversion coefficient calibration

Then we change the attitude of the hexapod. For each deviation angle of the hexapod, we calculate the real laser spot position. Ideally, rotation of the z_H-axis of the hexapod will only change the incident angle of the receiving beam in the yaw direction, while rotation of the x_H-axis of the hexapod will only change the incident angle of the receiving beam in the pitch direction. However, in the experiment, the rotation coordinate of the hexapod and the coordinate of the optical platform may have an offset. The rotation of one axis may cause the laser spot position changing in both directions. Make the rotation of the x_H-axis as an example. The rotation angle varies from -600 μrad to 600 μrad. Figure 11(a) shows the relationship between the rotation angle and the laser spot position in the y_C-direction of the CMOS, while Fig. 11(b) shows such relationship for the x_C-direction of the CMOS. The blue curve is the linear fitting curve. It can be seen that the coupling between the two directions is truly exist. The angle-position conversion coefficients of the CMOS camera can be obtained by calculating the linear fitting coefficient. Based on the above results, the conversion coefficients are calculated as $k_{x-y} \approx 7.76 \times 10^{-3}$ pixel/μrad, $k_{x-x} \approx 1.806 \times 10^{-4}$ pixel/μrad, respectively. Similarly, the conversion coefficients with z_H-axis rotation can be calculated as $k_{z-x} \approx -8.85 \times 10^{-3}$ pixel/μrad, $k_{z-y} \approx 5.104 \times 10^{-4}$ pixel/μrad, respectively. Therefore, in the experiment, the relationship between the tested laser spot position and the deviation angle is given by,

$$\begin{pmatrix} \theta_x \\ \theta_z \end{pmatrix} = \begin{pmatrix} x_{ref} - x_{real} \\ y_{ref} - y_{real} \end{pmatrix} \cdot \begin{pmatrix} k_{x-x} & k_{z-x} \\ k_{x-y} & k_{z-y} \end{pmatrix}^{-1}, \tag{20}$$

where, θ_x and θ_z represent the deviation angle of the hexapod in the x-direction and the z-direction respectively, x_{real}, y_{real} is the tested laser spot position.

The phase-angle conversion coefficient of the DWS signal can be obtained with the same method. The linear fitting results shows that $k_{ud} = 1621$ rad/rad, $k_{rl} = 1592$ rad/rad.

4.3. Laser acquisition experimental results

After the calibration process, we arbitrarily move the position of P1 and P2 to simulate the initial state before acquisition. At first, the FSM scans over the uncertainty cone of the P1. At a certain time, the CMOS camera receives the laser spot with enough power. Then the FSM stops scanning.

Optics EXPRESS

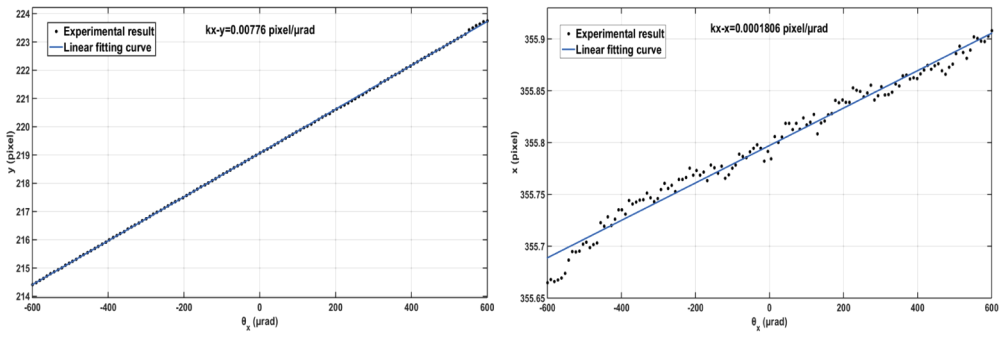

Fig. 11. (a) The relationship between the rotation angle of the x_H-axis θ_x and the spot position in the y-direction of the CMOS surface. (b) The relationship between the rotation angle of the x_H-axis θ_x and the spot position in the x-direction of the CMOS surface.

The QPD detects the interference signal and calculates the DWS signal continuously. The results at this time is regard as the initial deviation angle of the P1 line of sight. Make the DWS signal of up and down quadrants as an example, Fig. 12 shows the experimental results. For convenient comparison of the laser acquisition effect, we draw the DWS results before acquisition and after acquisition in the same figure. The DWS signal of the initial state corresponds to the sampling points $n_c \in (0, 1 \times 10^4)$. By calculating the mean value and dividing the phase-angle conversion coefficient, the initial deviation angle can be calculated as 241.6 μrad.

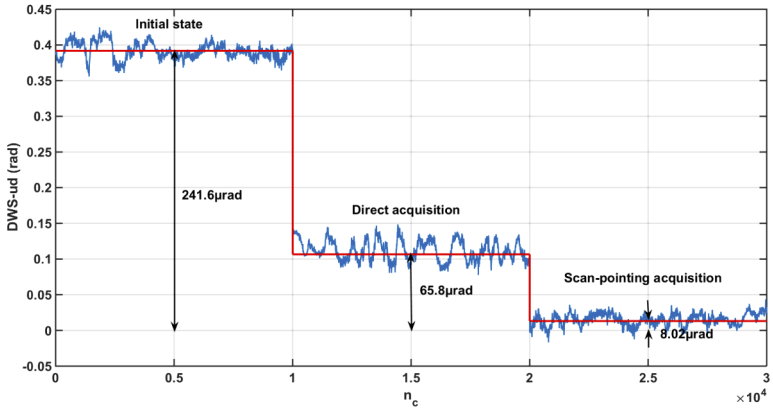

Fig. 12. Diagram of comprehensive experimental results. The DWS signal of the initial state corresponds to the sampling points $n_c \in (0, 1 \times 10^4)$. The DWS signal after direct acquisition process corresponds to the sampling points $n_c \in (1 \times 10^4, 2 \times 10^4)$. The DWS signal after scan-pointing acquisition process corresponds to the sampling points $n_c \in (2 \times 10^4, 3 \times 10^4)$.

Then the laser acquisition process is simulated. Firstly, the direct acquisition scheme is carried out. As the CMOS camera has already received a laser spot with enough power, no other scanning process is needed. The attitude of the hexapod is adjusted based on the laser spot center positioning result and the formula (5). The QPD detects the DWS after direct acquisition to verify the acquisition precision. The results are also shown in Fig. 12 corresponding to $n_c \in (1 \times 10^4, 2 \times 10^4)$. It can be seen that the deviation angle is suppressed to 65.8 μrad with the help of the acquisition simulation system. The acquisition precision can fulfill the requirement of 80 μrad. However, the residual deviation angle is far larger than the theoretical precision and very

Optics EXPRESS

close to the requirement. To improve the robustness of the laser acquisition experimental system, the residual deviation angle should be further suppressed. Then the scan-pointing acquisition scheme is carried out. As introduced in section 3.3, the transmitting laser beam is adjusted to point to the aperture center before laser acquisition. The sampling points of $n_c \in (2\times10^4, 3\times10^4)$ in Fig.12 presents the DWS read out after the scan-pointing acquisition process. It can be seen that after laser acquisition process, the deviation angle is about 8.02 μrad. Compared with the direct acquisition results, the deviation angle is further suppressed.

The residual noise mainly comes from the DWS readout error. As the experimental system is exposed in the atmosphere, the air turbulence and the temperature fluctuation will influence the optical path length of the transmitting laser. As a result, the interference signal and the DWS signal are also affected. To measure the fluctuation of the DWS signal, we firstly adjust the hexapod to make the DWS value approximately equal to zero. Then, the QPD continuously detects the DWS signal for more than 3×10^4 sampling points (500 s). Figure 13 shows the results of the up and down quadrants. The RMS value of the results is 0.0083 rad. Correspondingly, the angular measurement fluctuation of the DWS technique is calculated as approximately 5 μrad. Comprehensively considering the air turbulence and the in-flat top properties, the DWS technique can be used to test the acquisition precision in the experiment but involves measurement error of sub-10 μrad magnitude.

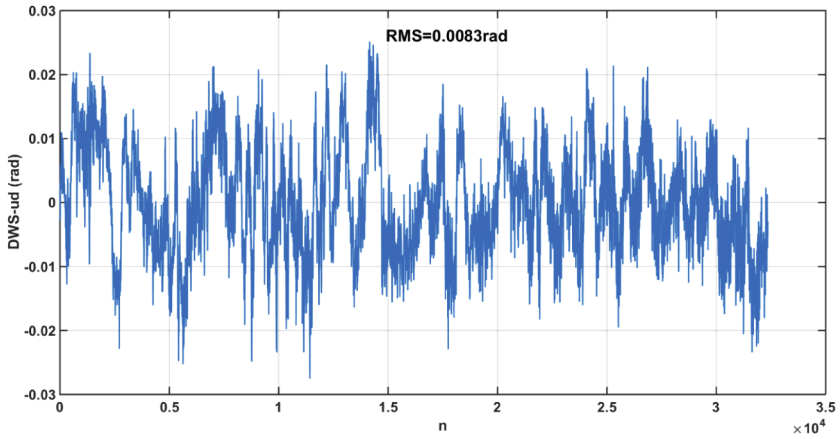

Fig. 13. Continuous experimental results of the up and down quadrants DWS signal.

To verify the feasibility of the laser acquisition experimental system, other experiments with various relative positions of P1 and P2 are also carried out. All the experimental results shows that the acquisition precision at the CMOS camera can reach sub-10 μrad magnitude. The requirement of the Taiji/LISA can be fulfilled. The experiment system realizes methodological demonstration of the laser acquisition scheme. The results offer the experimental foundation and theoretical basis for the acquisition system of the Taiji program.

5. Summary

In this paper, according to the requirements of the Taiji program for laser acquisition system, a laser acquisition ground-based simulation experimental system is designed and constructed. The experimental system restores the actual laser acquisition system from three aspects: optical path, acquisition accuracy and acquisition process. The experimental system also takes the coupling between laser acquisition process and laser pointing process into consideration. We synthetically consider the flat-top beam simulation and scanning range simulation in system parameter design. We also analyse the limiting factors to the acquisition precision in ground-based

Optics EXPRESS

experimental system. With limited beam transmitting distance of 1 m, the intensity distribution is in-homogeneity while the beam transmitting direction is in-consistency within the aperture area. The in-flat top properties of the receiving beam bring 100 μrad magnitude angular measurement error to the acquisition system as well as 10 μrad magnitude read out error to the DWS signal. For dealing with the problem, a scan-pointing acquisition scheme is introduced in the experiment. Before laser acquisition, the transmitting beam is adjusted to point to the aperture center with the help of a scanning strategy. At this time, the influence of the in-flat top properties of the receiving beam greatly reduced. The experimental results show that the acquisition precision of sub-10 μrad magnitude can be achieved, which can fulfill the requirement of the Taiji program. The experimental system provides a theoretical basis for the design of the laser acquisition system and realizes methodological demonstration of the laser acquisition scheme of the Taiji program.

Funding. Chinese Academy of Sciences (XDA1501800003, XDA1502070304, XDA1502070902).

Disclosures. The authors declare no conflicts of interest.

References

1. W. Hu and Y. Wu, "The Taiji Program in Space for Gravitational wave physics and the nature of Gravity," Natl. Sci. Rev. **4**(5), 685–686 (2017).
2. Z. Luo, Z. Guo, and G. Jin, "A brief analysis to Taiji: science and technology," Results Phys. **16**, 102918 (2020).
3. Z. Luo, Y. Wang, and Y. Wu, "The Taiji program: A concise overview," Prog. Theor. Exp. Phys. (2020).
4. K. Danzmann, The LISA Study Team, "LISA: laser interferometer space antenna for gravitational wave measurements," Classical Quantum Gravity **13**(11A), A247–A250 (1996).
5. J. O, B. P, and C. M, "NGO assessment study report (Yellow Book)," Cosmol. Extra-Galactic Astrophys. (2012).
6. G. D. Fletcher, T. R. Hicks, and B. Laurent, "The SILEX optical inter-orbit link experiment," The Inst. Electr. Eng. **3**, 273–279 (1991).
7. K. Abich, "In-Orbit Performance of the GRACE Follow-on Laser Ranging Interferometer," Phys. Rev. Lett. **123**(3), 031101 (2019).
8. D. Schutze, G. Stede, and V. Muller, "Laser beam steering for GRACE Follow-On intersatellite interferometry," Opt. Express **22**(20), 24117–24132 (2014).
9. D. M. R. Wuchenich, C. Mahrdt, and B. S. Sheard, "Laser link acquisition demonstration for the GRACE Follow-On mission," Opt. Express **22**(9), 11351–11366 (2014).
10. F. Cirillo, "Controller Design for the Acquisition Phase of the LISA Mission using a Kalman Filter," Ph.D. thesis, Pisa University (2007).
11. F. Cirillo and P. F. Gath, "Control System Design for the Constellation Acquisition Phase of the LISA Mission," *7TH INTERNATIONAL LISA SYMPOSIUM* (2008).
12. R. Gao, H. Liu, Z. Luo, and G. Jin, "Introduction of Taiji Program Laser Pointing Scheme," Chin. Opt. **12**(3), 425–431 (2019).
13. E. Morrison, B. J. Meers, D. I. Robertson, and H. Ward, "Automatic alignment of optical interferometers," Appl. Opt. **33**(22), 5041–5049 (1994).
14. E. Morrison, B. J. Meers, D. I. Robertson, and H. Ward, "Experimental demonstration of an automatic alignment system for optical interferometers," Appl. Opt. **33**(22), 5037–5040 (1994).
15. G. Hechenblaikner, "Measurement of the absolute wavefront curvature radius in a heterodyne interferometer," J. Opt. Soc. Am. A **27**(9), 2078–2083 (2010).
16. Y. Dong, "Inter-satellite Interferometry: Fine Pointing and Weak-light Phase-locking Techniques for Space Gravitational Wave Observatory," Ph.D. thesis, The University of Chinese Academy of Sciences (2015).
17. T. T. Hyde, P. G. Maghami, and S. M. Merkowitz, "Pointing acquisition and performance for the laser interferometry space antenna mission," Classical Quantum Gravity **21**(5), S635–S640 (2004).
18. P. G. Maghami, T. T. Hyde, and J. Kim, "An acquisition control for the laser interferometer space antenna," Classical Quantum Gravity **22**(10), S421–S428 (2005).
19. D. I. Robertson, E. D. Fitzsimons, and C. J. Killow, "Construction and testing of the optical bench for LISA Pathfinder," Classical Quantum Gravity **30**(8), 085006 (2013).
20. E. D. Fitzsimons, J. Bogenstahl, and J. Hough, "Precision absolute positional measurement of laser beams," Appl. Opt. **52**(12), 2527–2530 (2013).
21. R. Gao, H. Liu, Z. Luo, and G. Jin, "High-precision laser spot center positioning method for weak light conditions," Appl. Opt. **59**(6), 1763–1768 (2020).